Electrodeposition of Adherent Submicron to Micron Thick Manganese Dioxide Films with Optimized Current Collector Interface for 3D Li-Ion Electrodes

Marina Y. Timmermans,[a,z] Nouha Labyedh,[a,b,*] Felix Mattelaer,[c,*] Stanislaw P. Zankowski,[a,b,*] Stella Deheryan,[b] Christophe Detavernier,[c] and Philippe M. Vereecken[a,b,,z]**

[a]*IMEC, 3001 Leuven, Belgium*
[b]*Centre for Surface Chemistry and Catalysis, University of Leuven (KUL), 3001 Leuven, Belgium*
[c]*Department of Solid State Sciences, Ghent University, 9000 Gent, Belgium*

Three-dimensional (3D) configuration of high-performance energy storage devices has been the subject of ongoing investigations targeting their integration in autonomous microelectronic systems. In this study we demonstrate a route toward the realization of high capacity cathode material for 3D thin-film lithium-ion (Li-ion) batteries. Electrolytic manganese dioxide (EMD) film can be applied as a Li-ion intercalation electrode upon its conversion to lithium manganese dioxide ($LiMn_2O_4$ or LMO) by solid-state reaction. The main challenges of depositing thicker EMD film directly on the current collector often lay in achieving a good film adhesion and preventing oxidation of non-noble current collectors such as TiN, Ni. To improve the adhesion of the EMD films we modify the surface of the current collector by means of thin-film or seed layer coatings, which also prevent the oxidation of the underlying current collector substrate during the anodic deposition process. As a result submicron to micron thick EMD films with good adhesion were deposited on various current collectors. The acidity of the electrolyte solutions was varied depending on the type of the surface coating or current collector used. The mechanism of the EMD film growth and morphology on different substrates was examined. Compatibility of the proposed current collector interface modification for the electrodeposition of conformal thick EMD films on high-aspect ratio microstructures was demonstrated. A method of EMD film conversion to LMO at low-temperature on different substrates was shown as the path toward their application in 3D Li-ion batteries.

Manuscript submitted August 16, 2017; revised manuscript received October 24, 2017. Published November 14, 2017.

Emerging electronic microsystems such as autonomous sensor systems for smart environments, body area networks, biomedical devices for lab-on-chip diagnosis and implants require onboard microstorage. For such applications the development of powerful, small and intrinsically safe batteries with sufficient storage capacity and long lifetime is critical. The key enabler to address the energy and power demands of footprint-limited autonomous devices is a three-dimensional (3D) configuration of energy storage devices such as lithium-ion (Li-ion) batteries and supercapacitors, where thin-film material is coated on a microstructured current collector.[1–3] The surface area enhancement associated with 3D structuring not only provides more material for the same footprint, but also increases the interface between the active electrode material and the electrolyte, thus reducing the cell resistance and providing more surface for reversible insertion and extraction of Li ions.[4] As opposed to nanostructured electrode configuration, 3D microstructuring of energy storage devices allows to increase the thickness of active layers for improved areal capacitance. However, conformal deposition of films with good adhesion on industrially-relevant current collectors is an essential requirement and still remains a challenge.

Manganese dioxide (MnO_2) has been widely explored for energy storage systems as a potential cathode material in rechargeable batteries and supercapacitors owing to its lower cost, environmental benignity and electrochemical properties. Electrodeposition is the primary method to prepare MnO_2 typically in the γ-MnO_2 form, which is commonly used today in primary alkaline and lithium batteries.[5] This phase of MnO_2 is referred to as electrolytic manganese dioxide or EMD. Typically, EMD is fabricated by anodic electrodeposition of several micrometer thick layers on titanium anodes from hot (80–98°C) acidic electrolytes, followed by its mechanical removal from the anode and grounding it into powders to be used as electrodes.[6,7] Electrodeposition in one of the preferred techniques for MnO_2 preparation due to its processing simplicity, scalability and possibility to obtain conformal EMD deposition on high aspect ratio substrates. Therefore, electrodeposition of MnO_2 has also been explored for 3D thin-film storage devices, being electric double-layer capacitors or Li-ion batteries. In this work, thick MnO_2 films are deposited directly onto the surface of the current collector. The thickness of such films ranges from 250 nm to >1 μm for the optimized current collector interface. For 3D battery applications, the thickness of the EMD film on microstructures with an area enhancement of 20–40x (see Figure S1) should be close to 500 nm in order to match the capacity requirements of commercial Li-ion batteries for high-power applications (60–120 mAh/cm^3).[8,9] At the same time, the increase of the film thickness should not compromise the electrochemical performance of the material.[10] The main challenges of depositing thicker EMD film directly on the current collector often lay in achieving a good film adhesion, which can be challenged by the dissolution or passivation of the current collector in an acidic environment during the anodic EMD deposition. This typically results in delamination of the EMD film deposits or limitations in their electrochemical activity due to the oxidation of the underlying current collector. Various substrates have been used for the electrodeposition of MnO_2 material for their use in electrochemical capacitors or batteries.[11–14] The importance of substrate variation for the EMD deposition mechanism has been highlighted but not given much attention.[11]

In this work we propose ways to obtain thicker and well-adherent EMD films on technologically-relevant but oxidizable materials such as titanium nitride (TiN) and nickel (Ni) which are often used as current collectors in energy storage applications. TiN is a common material used as a diffusion barrier on silicon. For thin film Li-ion batteries, in particular, TiN was shown to be a good Li-ion diffusion barrier and can also be used directly as an electrode material.[15] Therefore, TiN is the focus support material in this work, but the findings are relevant for other oxidizable substrates. We explore different substrate coatings including carbon nanostructures, ultra-thin MnO_2 seed layer and nickel (Ni) film for the deposition of thicker EMD films. The latter can also be used as a 3D current collector on its own. The physical properties of the deposited films and the deposition mechanism associated with the substrate and electrolyte acidity variation is discussed. The applicability of as-deposited EMD films as Li-ion intercalation electrodes in thin-film batteries is demonstrated by converting EMD to lithium

*Electrochemical Society Student Member.
**Electrochemical Society Member.
[z]E-mail: marina.timmermans@imec.be; philippe.vereecken@imec.be

manganese dioxide ($LiMn_2O_4$ or LMO) films with higher capacity. Finally, conformal deposition of thick EMD films on 3D microstructures is shown paving a way toward their application in 3D energy storage devices.

Experimental

EMD film deposition.—EMD films were anodically electrodeposited using a three electrode cell configuration with Pt mesh counter electrode and Ag/AgCl/3M NaCl reference electrode (BASi analytical, 0.22 V vs SHE). An aqueous solution of 0.3M $MnSO_4 \cdot H_2O$ (98.0–101.0%, Alfa easer) and 0.3M H_2SO_4 (96%, OMG) was used for the deposition of manganese dioxide on most of the studied substrates at room temperature (20–25°C). For comparative electrochemical measurements also an indifferent electrolyte solution of 0.3M Na_2SO_4 (99.0%, Sigma Aldrich) and 0.3M H_2SO_4 was applied. EMD on Ni-coated TiN layer was prepared from an aqueous solution of 0.5M $MnSO_4 \cdot H_2O$ (98.0–101.0%, Alfa easer) and 0.5M CH_3COONa (ReagentPlus, 99.0% Sigma Aldrich) with an addition of ∼10 wt% ethanol for wetting improvement.[16] All the depositions were carried out galvanostatically at a constant current density of 0.5 mA/cm^2 for different time periods, obtaining variable film thickness. For the deposition of EMD on Ni using acetate based electrolyte an additional nucleation step of high current density of 2.5 mA/cm^2 for 1–8 sec was added prior to the film growth at 0.5 mA/cm^2. In the present study we focus on film deposition carried out at room temperature. After the deposition EMD samples were annealed at 350°C in N_2 atmosphere (ambient pressure) to remove the water content within the film structure.[5]

Substrate materials.—Planar silicon wafers (n type) coated with a 60 nm TiN layer were used for most of the results presented here. TiN layer was sputtered from a Ti target in a N_2 atmosphere (Applied Endura Extensa TTN). Graphitic carbon nanosheet (CNS) layers (20–70 nm) were used as one of the TiN coating materials, further referred to as C/TiN substrate. CNS layers were grown in a capacitively coupled PECVD reactor with a 13.56 MHz RF generator (Oxford Instruments plasma technology UK NANOCVD) introducing C_2H_2-H_2 (1:10) for 2–3 minutes at 800°C, 0.45 Torr and RF power of 300 W[9]. Atomic layer deposition (ALD) was employed for the growth of ultrathin MnO_2 seed layers (2.2–4.6 nm) on top of the TiN current collector. Tris(2,2,6,6-tetramethyl-3,5-heptanedionato)manganese ($Mn(thd)_3$) was used as a manganese precursor, and ozone was used as an oxygen source.[17,18] ALD films were grown in a home-built stainless steel high-vacuum ALD reactor with a base pressure of 10^{-7} mbar at a substrate temperature of 180°C, which was chosen to be well within the ALD window.[19] The number of ALD cycles was optimized to the required thickness. A layer of Ni (100 nm) was deposited on TiN from a Ni target in a PVD advanced low pressure source chamber (Applied Endura Extensa TTN). For 3D silicon microstructures conformal TiN coating was deposited by means of ALD (thermal process at 390°C using $TiCl_4$ as precursor) and Ni was electroplated (galvanostatic deposition at a fixed effective current density of −10 mA/cm^2, using 0.62 M Ni sulfamate with H_3BO_3).

Material analysis.—Different techniques have been applied in this work for material analysis. The morphology and thickness of as-deposited EMD films was characterized by scanning electron microscopy (SEM) using NOVA 200 microscope for standard measurements (up to 100,000x magnification) and a Hitachi SU8000 for higher resolution measurements (up to 300,000x magnification). Rutherford Back Scattering (RBS) measurements were carried out using He^+ beam of 1.523 MeV, with scattering angle 170°, and sample tilt angle of 11°. Ex-situ X-ray diffraction (XRD) with X'pert Panalytical using Cu Kα radiation (8.04 keV) in grazing incidence configuration was applied for the analysis of thin film crystallinity. In-situ XRD was performed in a Bruker D8 Discovered using Cu Kα radiation and a linear detector. The film crystallinity was monitored in-situ, measuring the samples during annealing in a home-built annealing chamber with controlled ambient and temperatures.[20] X-ray photoelectron spectroscopy (XPS) was performed for elemental composition measurements using a monochromatized Al Kα X-ray source (1486.6 eV) and a spot size of 400 μm. For the chemical composition analysis, measurements were carried out in Angle Resolved mode using a Theta300 system from Thermo Instruments. 16 spectra were recorded at exit angles between 22° and 78° as measured from the normal of the sample.

Electrochemical characterization.—Electrochemical characterization of as-deposited EMD films and EMD films converted to LMO was performed in a three-electrode Teflon cell setup with Li metal ribbons as reference and counter electrodes. The reference electrode compartment was connected to the main cell compartment through a Luggin capillary (∼1 mm above surface). The Li-ion electrolyte solution consisted of 1M $LiClO_4$ (99.99%, Sigma Aldrich) dissolved in propylene carbonate (99.7%, Sigma Aldrich). During characterization the electrochemical cell was placed inside an argon filled glove box (Pure lab, PL-HE-4GB-1800, <1 ppm O_2 and H_2O level). An AUTOLAB potentiostat PGSTAT204 controlled by Nova 1.9 software (Metrohm) was utilized for these measurements.

Results and Discussion

Improved adhesion of thick EMD on TiN with C and MnO_2 surface coating.—Electrodeposition of MnO_2 from acidic electrolytes, typically being aqueous baths of manganese sulfate ($MnSO_4$) and sulfuric acid (H_2SO_4), has been widely reported.[10] In our previous work, EMD films were electrodeposited from acidic $MnSO_4$ baths on planar platinum (Pt) coated substrates.[5] EMD films grown from acidic electrolytes on different substrates were shown to be highly porous (∼50% porosity) consisting of a network of interconnected 5–10 nm nanoparticles.[5,9] However, a very poor adhesion of the EMD films electrodeposited on the noble metal (Pt) coated substrate was observed. The maximum thickness of well-adherent EMD films was limited to 150 nm, with thicker deposits delaminating due to the mechanical film stress.[5] Additionally Pt-group metals do not comply with cost-effective application targets. In that respect, electrically conductive non-noble TiN is a suitable current collector which, at the same time, is a good Li-ion diffusion barrier.[15] However, the application of EMD films directly on TiN is limited, since TiN oxidation occurs in approximately the same potential range as the anodic electrodeposition of EMD. A linear sweep voltammogram of MnO_2 electrodeposition from an acidic (solid red) and an indifferent (dashed blue) electrolyte solutions using a TiN substrate is shown in Figure 1a. The presence of an anodic current peak at +1.6 V in an indifferent electrolyte solution indicates the electro-oxidation of TiN to $TiON_x$, which forms a passivating layer of ∼1.5 nm (as estimated from the charge under the current peak) and inhibits the oxygen evolution.[9] In the reverse scan the current becomes nearly zero and no cathodic current is observed due to the formation of an electronically blocking interface between the current collector and the EMD film. Interestingly, this interfacial oxide does not fully block the anodic oxidation reaction as even thicker EMD deposits could be achieved for longer deposition times. An example of 380 nm thick EMD film on TiN is shown in Figure S2a. However, these thicker films deemed inactive with no typical Li-ion intercalation peaks observed (see Figure S2b). In fact, on TiN substrate EMD films of only less than 50 nm thick were found to be electrochemically active as shown in our earlier studies.[5] This indicates that with the extended oxidation of TiN, the interfacial oxide starts blocking the cathodic Li-ion intercalation reaction, whereas for short deposition times the oxidized TiN surface still allowed sufficient electronic contact between TiN ad MnO_2. This seems counter intuitive at first as TiO_2 is n-type semiconductor and one would expect the anodic reaction to be blocked instead. However, this can be explained by the blocking of electrons with the formation of a p-n junction at the $TiON_x/MnO_2$ interface. This phenomenon was confirmed by plating thicker EMD films on thin ALD TiO_2 coated TiN films (an example

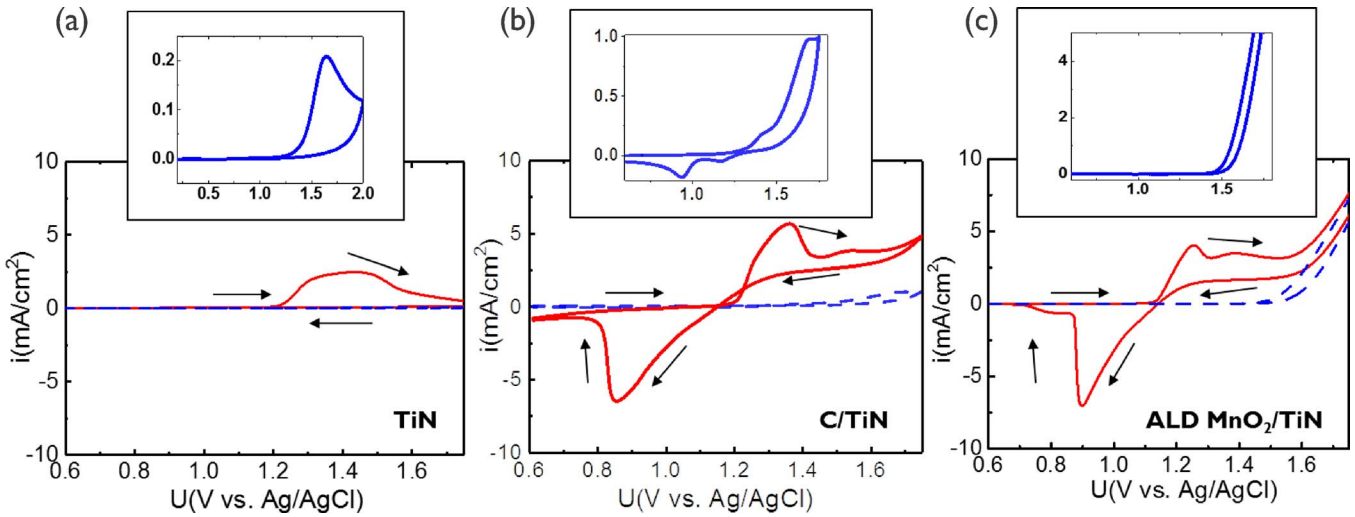

Figure 1. (a) Cyclic voltammograms in a sulfuric acid based Mn(II) solution (0.3M $MnSO_4$ and 0.3M H_2SO_4) [solid red lines] and an indifferent electrolyte solution (0.3M Na_2SO_4 and 0.3M H_2SO_4) [dashed blue lines and insets] on (a) TiN substrate, (b) carbon nanosheets coated TiN (C/TiN) and (c) seed layer ALD MnO_2-coated TiN substrates. The voltammograms were recorded at a polarization rate of 20 mVs^{-1}, starting from an open-circuit potential and going to more positive potentials (arrows indicate the scan direction).

of 250 nm thick EMD film is shown in Figure S3a), which exhibited no electrochemical performance (Figure S3b).

In order to circumvent the issue of the substrate oxidation, we have proposed to coat the TiN substrate with a layer of short carbon nanosheets (CNS) with a sheet thickness ranging from a few to tens of nanometers[9] (Figure 2). We believe that the application of such nano-rough graphitic carbon improves the EMD adhesion due to the formation of covalent-like bonds between MnO_2 particles and surface groups of defective carbon (C-O bonds). Well-adherent EMD films exceeding 1 μm were electrodeposited on top of carbon (C)-coated TiN substrates (Figure 2b). However, we recognize that for certain applications where elevated temperatures are required, the use of a carbon coating might impose certain temperature limitations on further stack processing.

Therefore, we suggest another approach to avoid the oxidation of the substrate during the electrochemical deposition. It involves coating an oxidizable substrate such as TiN with a very thin MnO_2 seed layer by e.g. ALD. It was observed that the presence of the so-called MnO_2 seed layer improves the mechanical adhesion of the EMD film due to the formation of native covalent bonds between Mn-O and Mn-O. Thick EMD films up to ~1 μm were prepared on top of a planar substrates coated with 2–4 nm MnO_2 seed layer (Figure 3). The ability of such ultrathin MnO_2 seed layer to protect TiN from oxidation was confirmed by in-situ XRD analysis (Figure S4).

Figure 1b and Figure 1c show the electrochemical behavior of C-coated TiN and ALD MnO_2-coated TiN substrates in $MnSO_4$ solution (solid red) and an indifferent electrolyte solutions (dashed blue and insets). The behavior in the indifferent electrolyte solutions is substrate dependent. For the C/TiN substrate as shown in Figure 1b, an anodic peak at ~1.4 V vs Ag/AgCl is visible which can be attributed to the carbon oxidation. However, the onset of oxygen evolution and the presence of cathodic current in the reverse scan indicates that graphitic carbon coating prevents the passivation of the TiN substrate. It is interesting to note that oxygen evolution reaction occurs somewhat earlier at ALD MnO_2-coated substrate (Figure 1c) where the MnO_2 seed layer is playing an important catalytic role which is a subject of our separate study.[21]

The electrochemical behavior in a Mn-containing electrolyte solution is very similar for both C/TiN and ALD MnO_2/TiN substrates. Clear anodic current peaks of 5.7 mA/cm^2 at 1.36 V vs Ag/AgCl for the C/TiN substrate and 4.1 mA/cm^2 at 1.25 V vs Ag/AgCl for the MnO_2/TiN substrate are distinguishable. These peaks are associated with the formation of an EMD film, which inhibits further deposition kinetics due to nearly insulating nature of the film. However, since the EMD film is porous, growth of the film still continues on the substrate due to the steady-state diffusion of the reagent through the pores of the film. That is well visible in the reverse scan plateau of Figures 1b–1c. For the uncoated TiN substrate a continuous oxidation of TiN is occurring simultaneously with the growth of EMD on top, as visible from Figure 4a from the constantly growing potential with the plating time. Stable deposition potential is observed for the EMD growth on top of the coated TiN substrates (Figures 4a, 4b).

Mechanism of EMD deposition.—A number of fundamental studies have focused on understanding the EMD deposition mechanism in detail, typically on a Pt substrate.[10,11,22,23] The general mechanism is

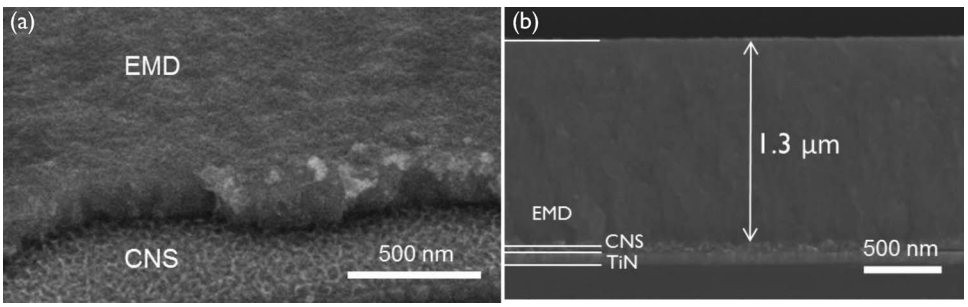

Figure 2. (a) Tilted and (b) cross-sectional SEM images of EMD on C/TiN, i.e. TiN coated with a layer of carbon nanosheets (CNS). EMD films were grown by galvanostatic deposition at 0.5 mA/cm^2 for (a) 400 s and (b) 1300 s using an aqueous bath of manganese sulfate ($MnSO_4$) and sulfuric acid (H_2SO_4).

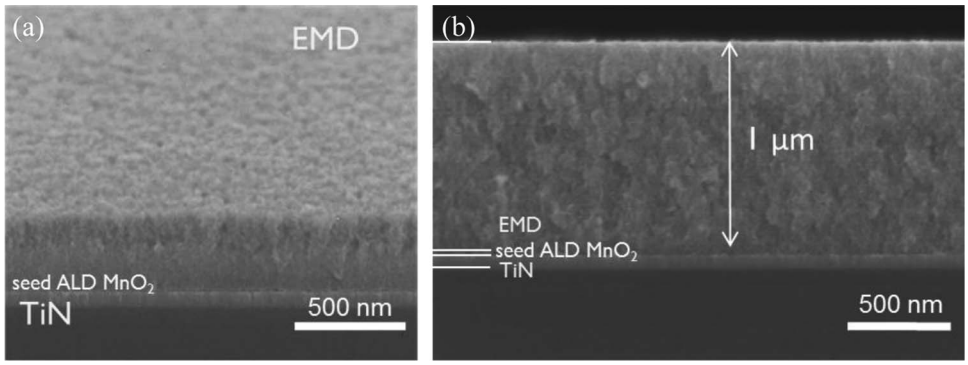

Figure 3. (a) Tilted and (b) cross-sectional SEM images of EMD on TiN coated with a thin ALD MnO_2 seed layer (~3.6 nm ALD MnO_2/TiN). EMD films were grown by galvanostatic deposition at 0.5 mA/cm^2 for (a) 400 s and (b) 1000 s using an aqueous bath of manganese sulfate ($MnSO_4$) and sulfuric acid (H_2SO_4).

agreed to go via the electrochemical oxidation of the solvated Mn^{2+} forming soluble Mn^{3+} intermediate. The electrolyte acidity influences the Mn^{3+} stability, which can further either diffuse out from the electrode surface to the bulk of the solution (initially) or precipitate as a passivating MnOOH layer. In the latter case, oxidation of MnOOH to form MnO_2 needs to happen to open up a site for the reaction to continue, which was identified as the limiting factor in the growth process.[11] The MnO_2 formation mechanism is as follows:

$$Mn^{2+}(aq) \rightarrow Mn^{3+}(aq) + e^- \quad [1]$$

$$Mn^{3+}(aq) + 2H_2O \leftrightarrow MnOOH(s) + 3H^+ \quad [2]$$

$$MnOOH(s) \rightarrow MnO_2(s) + H^+ + e^- \quad [3]$$

This deposition pathway is characteristic for the case when the acid concentration in the electrolyte solution is lower and $Mn^{3+}{}_{(aq)}$ ions have lower stability.[11] The free Mn^{3+} ions can disproportionate in the solution according to:

$$2Mn^{3+}(aq) + 2H_2O \leftrightarrow Mn^{2+}(aq) + MnO_2(s) \quad [4]$$

which will be observed mostly under acidic conditions as under these conditions the formation of free Mn^{3+} is more prevalent according to Reaction 2.

The EMD film growth occurs predominantly at the substrate interface with the diffusion of ionic species through the porous EMD film, as schematically demonstrated in Figure 5. MnO_2 is a poor electronic conductor and would quickly passivate the electrode if it was formed as a dense film. However, the deposit is nanoporous and the electrode reaction can proceed near the original electrode surface with slower ionic transport through the pores. Transport includes $Mn^{2+}{}_{(aq)}$ travelling toward the current collector surface, where reaction occurs, and hydrated protons diffusing out of the nanoporous EMD structure (Figure 5). This bottom-up EMD growth mechanism enables the formation of thicker EMD films on poorly conducting or passivated current collector materials, like the earlier discussed oxidized TiN (Figure S2a), ALD TiO_2 coated TiN substrate (Figure S3a) as well as on ALD-grown MnO coated TiN substrate (Figure S5). With the increase of the EMD film thickness, a trend of porosity decrease was noticed, pointing toward film densification with increasing thickness.[5] This is attributed to the disproportionation of Mn^{3+} inside the pores as described in Equation 4, which leads to the densification of the EMD film over time (therefore, an increase in the deposition efficiency).

The morphology of the as-deposited EMD films is largely defined by the dominant growth mechanism which is directly related to the electrode surface composition and its catalytic activity toward Mn^{2+} oxidation. Due to the high catalytic activity of Pt, Mn^{2+} rapidly oxidizes forming an excess of Mn^{3+} at the Pt electrode interface at a short time and at low overpotentials.[23] Partial chemical dissolution of Mn^{3+} both lowers the deposition efficiency and induces the interface porosity. This link between the increased deposition efficiency and concurrent decrease of porosity as the EMD film thickness on Pt increases was experimentally observed in our earlier work.[5] High film porosity at the interface during the earlier deposition stage could lead to poor adhesion and observed delamination of EMD from a Pt substrate with the film thickness increase.[5] High EMD film porosity and delamination issues were also observed for the nickel (Ni) substrate using an acid-based electrolyte, as addressed in the next section. Figure 6a shows the deposition efficiency with respect to the

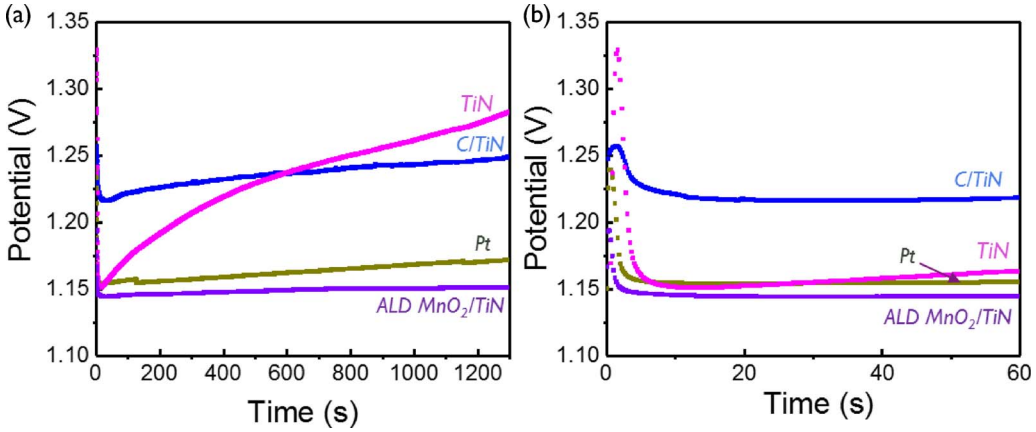

Figure 4. Galvanostatic deposition of EMD using $MnSO_4$ solution on different substrates for (a) 1300 s and (b) first 60 s.

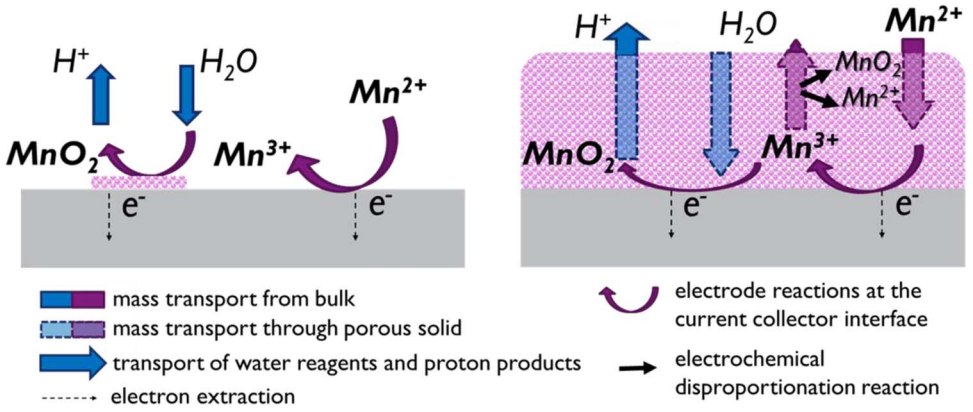

Figure 5. Schematics of the EMD growth mechanism.

charge density for the EMD deposition at the same current density on different substrates.

The deposition efficiency was estimated as the ratio of the equivalent MnO_2 film thickness determined from RBS (calculated from the quantity of Mn atoms assuming a dense MnO_2 film where the MnO_2 density is equal to 5.02 g/cm^3) to the theoretically expected MnO_2 film thickness derived from the deposition charge (using Faraday's law). The presence of the initial MnO_2 dense layer for seed ALD MnO_2-coated TiN substrates is taken into account in calculations. Lower deposition efficiency is related to the formation of soluble Mn^{3+} intermediates. As the EMD film grows, the deposition efficiency is observed to slightly increase which can be attributed to the increase of the ratio of Mn(IV) to Mn(III). Interestingly, the deposition efficiencies of Pt coated TiN substrates were consistently about 10% lower than that for C-coated and ALD MnO_2-coated TiN substrates. This indicates a larger partial charge transfer for the formation of Mn^{3+} and MnOOH on a Pt substrate (Pt > C > MnO_2). Subsequent structural changes during the solid-state oxidation of MnOOH to MnO_2 could have also contributed to building up stress in the EMD material and causing the observed delamination from a Pt substrate.[23] Deposition efficiency for the MnO_2 seed layer-coated substrate was found to be the largest of all the substrates. Note that the estimated deposition efficiency appears to be overestimated for all the EMD films due to the co-existence of Mn_2O_3 or MnOOH next to MnO_2 within the as-prepare EMD films, as confirmed by XRD analysis (Figure S6). That is apparent from the deposition efficiency for the thinnest EMD film on ALD MnO_2-coated substrate which exceeds the physically possible limit.

Since low deposition efficiencies were found to be linked to high EMD porosity, we further examine the porosity of EMD films on Pt/TiN, C/TiN and MnO_2/TiN substrates. Porosity of the films was estimated by comparing the equivalent RBS thickness of the MnO_2 films and the actual film thickness measured by cross-sectional SEM,[5] i.e.

$$Porosity = 100\% \cdot (1 - RBS\ film\ thickness/SEM\ film\ thickness) \quad [5]$$

The electrodeposited MnO_2 films were found to have similar porosity value of ~50% on average for Pt/TiN, C/TiN and MnO_2/TiN substrates (Figure S7). This confirms that the surface chemistry and surface morphology are at least partially responsible for the difference in adhesion between the electrodeposited MnO_2 film and the substrate. Figure 6b compares the maximum achieved thickness of EMD films on different substrates. The thickest EMD films were deposited on C-coated and seeded TiN substrates where the film deposition efficiency was the largest. This highlights the important role of the surface coating for the initial stages of EMD nucleation and growth. In this case MnO_2 is likely to form through the oxidation of MnOOH without significant Mn^{3+} desorption.[11] The presence of an ultrathin MnO_2 layer favors the formation of crystallite growth on top of the already deposited MnO_2 from the initial stages of the EMD deposition. This is confirmed by observing the potential change during the first seconds of EMD nucleation, where the smallest nucleation peak was observed for MnO_2-coated TiN (1.19V during the first 0.4 s of the deposition) as opposed to the uncoated TiN substrates exhibiting the largest nucleation peak (1.33V after 1.6 s of the deposition) as shown in Figure 4b.

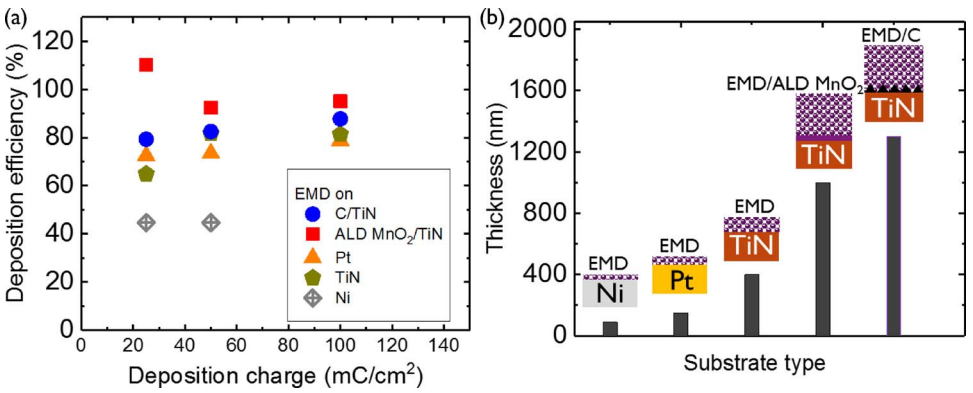

Figure 6. (a) Deposition efficiency as a function of deposited charge density for EMD films grown on different substrates at the same current density of 0.5 mA/cm^2. (b) Variation of maximum achieved EMD thickness from sulfuric acid based solution with respect to the substrate type of the current study.

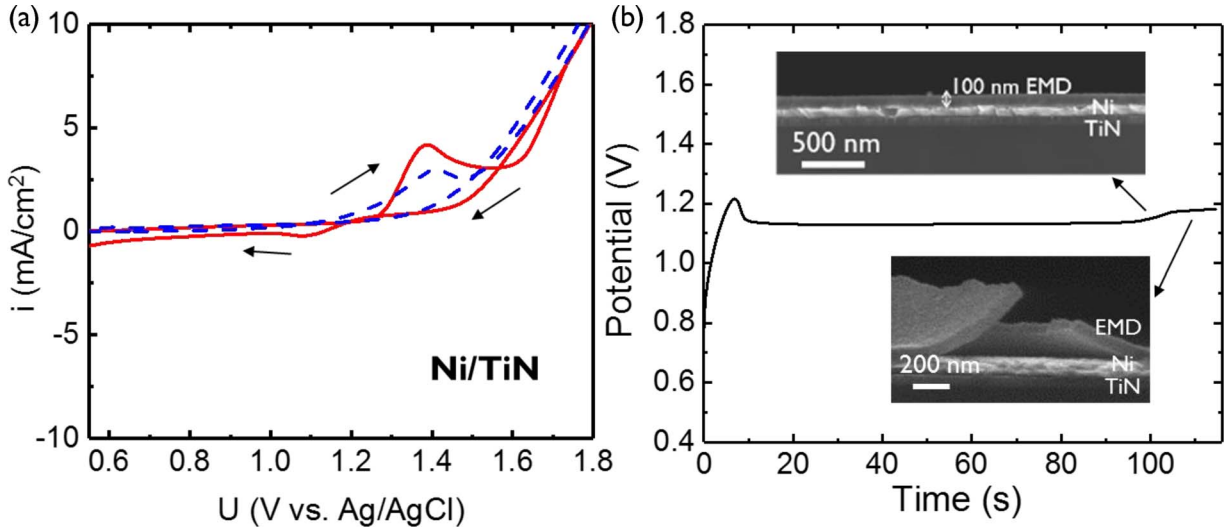

Figure 7. (a) Cyclic voltammograms in a sulfuric acid based electrolyte solution (0.3M $MnSO_4$+0.3M H_2SO_4) [solid red] and an indifferent electrolyte solution (0.3M Na_2SO_4+0.3M H_2SO_4) [dashed blue] on Ni-coated TiN substrate. (b) Potential (vs. Ag/AgCl) versus time for galvanostatic deposition of EMD thin films in electrolyte bath of 0.3M $MnSO_4$ and 0.3M H_2SO_4 on Ni/TiN at 0.5 mA/cm^2.

Thick EMD films on Ni-coated electrode.—Nickel (Ni) is an alternative current collector material which is stable in air owing to the surface-limited self-passivation and can be simply and controllably electrodeposited on high-aspect ratio structures for 3D device applications.[16] Ni is used as a current collector material itself and in this work it is a coating layer on top of TiN. Figure 7a shows cyclic voltammograms (CVs) in a sulfuric acid based $MnSO_4$ and indifferent electrolyte solutions. The presence of a small cathodic stripping peak confirms a small partial current for MnO_2 deposition. However, simultaneously to EMD deposition, partial Ni oxidation and concurrent slow dissolution of the NiO occurs in this process. Note that the surface of the Ni layer is already self-passivated at the start of the electrodeposition process. Indeed, if the potential is brought to −1 V vs. Ag/AgCl, the passivating NiO gets reduced and upon a positive scan, a strong anodic Ni dissolution current can be observed starting at −0.2 V vs. Ag/AgCl, as shown for example in the 2nd CV scan of Figure S9. The deposition of EMD films on Ni using acid-based electrolyte is possible at room temperature at very low current densities (∼0.5 mA/cm^2) when the NiO dissolution is inhibited by the growing EMD layer, but the thickness of this layer is limited to <100 nm (Figure 7b). The low deposition efficiency vs charge shown in Figure 6a for Ni-coated TiN substrate demonstrates that the partial current of parasitic Ni oxidation is significant, leading to a quick delamination of the EMD film grown on top. The as-grown EMD films were also found to be highly porous (Figure S7) which is partially responsible for their delamination together with the dissolution of NiO.

To overcome these problems, a neutral aqueous electrolyte of 0.5M $MnSO_4$ and 0.5M CH_3COONa with 10 wt% ethanol was used.[16] CVs were recorded for Ni in Mn-containing and indifferent electrolytes (Figure 8a). No significant oxidation peaks for Ni in an indifferent electrolyte were present, while the anodic oxidation peaks of Mn^{2+} to MnO_2 and cathodic reduction peaks of MnO_2 to MnOOH in a Mn-containing electrolyte are clear. Multiple anodic peaks are due to oscillations as a result of cyclic pH change related to buffering effect of acetate ions. Well-adherent EMD films up to 500 nm were deposited on a Ni substrate as shown in Figure 8b. Thicker deposits (>500 nm) could also be deposited but were observed to delaminate due to stress upon the subsequent EMD annealing step.

The morphology of the EMD film on Ni as a function of the deposition time was studied. Initially, a more open fibrous or sheet-like EMD morphology is obtained from the neutral bath which gradually densified with plating time. The densification is also apparent from the porosity of the films plated for different times, determined from RBS and SEM thickness (Figure 9a). The sheet like structure of the EMD film is shown in Figure 9b. Densification with plating time goes in line with the earlier discussed bottom-up EMD growth

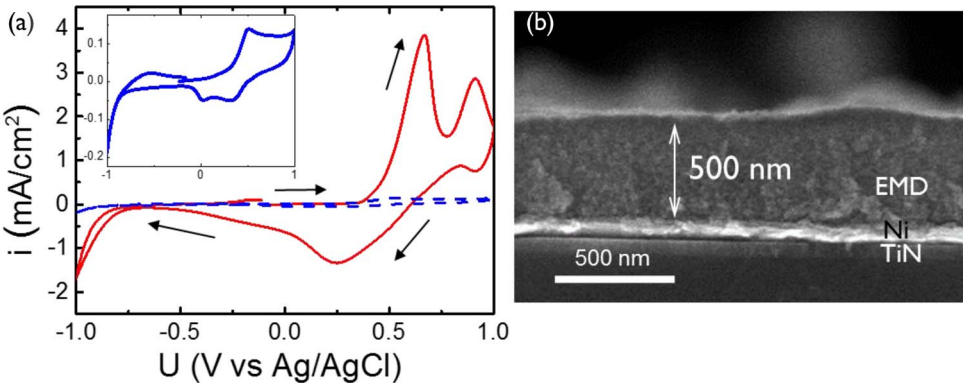

Figure 8. (a) Cyclic voltammograms in an acetate based electrolyte solution (0.5M $MnSO_4$ and 0.5M CH_3COONa with 10 wt% ethanol) [solid red] and an indifferent electrolyte solution (0.3M Na_2SO_4+0.5M CH_3COONa with 10 wt% ethanol) [dashed blue] on a Ni coated TiN substrate. (b) SEM of a ∼500 nm thick EMD film grown on a Ni coated TiN from an acetate based electrolyte solution.

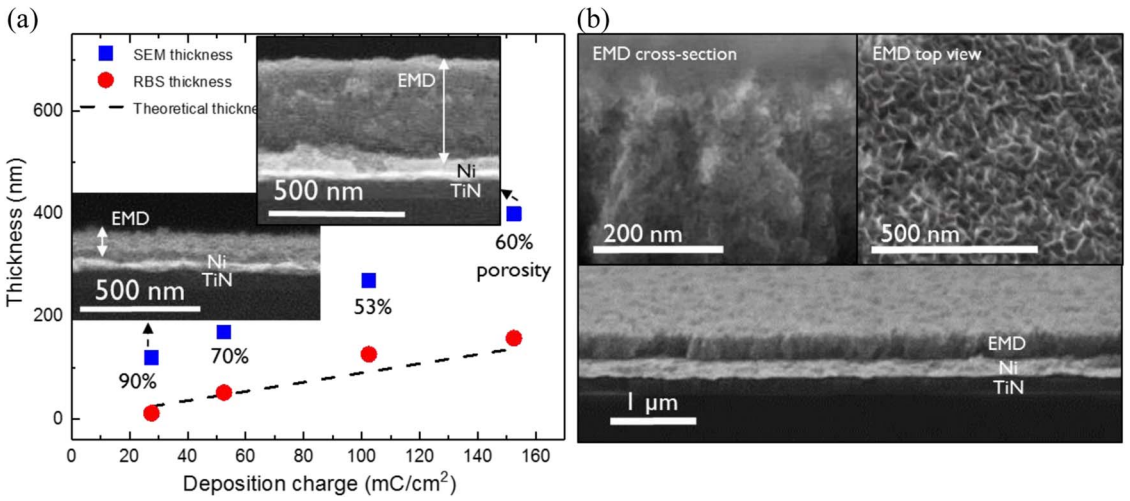

Figure 9. (a) EMD thickness variation with deposition charge density (at 0.5 mA cm^{-2}) obtained by SEM [blue squares], from RBS measurements [red circles] and theoretically expected from Faraday's law [black dashed]. Insets: cross- and top-view SEMs of 110 nm EMD film and 400 nm EMD film on Ni/TiN. (b) Cross-sectional and top view SEM view of the EMD film grown on Ni coated TiN for 200 s at 0.5 mA cm^{-2} using an electrolyte solution of 0.5M $MnSO_4$ and 0.5M CH_3COONa with 10 wt% ethanol.

mechanism. The MnO_2 electrodeposition reaction produces 4 H^+ cations per MnO_2 molecule. Similarly to the slow diffusion of Mn^{2+} from the bulk of the solution to the electrode surface through the nanoporous MnO_2 network, also the H^+ diffusion out of the MnO_2 layer is slowed down. As a result, the acidity inside the porous MnO_2 increases as the layer thickness increases. The increased acidity affects the electrodeposition mechanism and the partial current for Mn^{3+} (Reaction 4) will increase. The free $Mn^{3+}{}_{(aq)}$ at its turn has to diffuse out of the layer and the disproportionation into MnO_2 and $Mn^{2+}{}_{(aq)}$ (Reaction 4) increases with the film thickness. This $Mn^{3+}{}_{(aq)}$ disproportionation inside the pores results in the densification of the EMD film. The gradual densification is also supported by the variation of the film porosity which decreases with the increase of the plating time (Figure 9a).

The variation of deposition efficiency with deposition charge follows a similar trend as observed earlier for the EMD deposition using acid electrolyte. The calculated efficiency values of 100% or larger are attributed to the presence of other Mn oxidation states in the deposit. Indeed, XPS analysis of the EMD films on Ni/TiN could not exclude confirmed the presence of MnOOH or Mn_2O_3 or combination, since their peaks are overlapping in shape and position (Figure S8).

Conformal coating of thick MnO_2 films.—For electronically conductive coatings achieving conformal depositions is typically a challenge due to ion depletion in deep features, as for example demonstrated. in copper through-silicon vias technology.[24,25] In case of MnO_2 electrodeposition, the self-limiting nature of the oxide growth provides excellent conformality. The 3D-compatible deposition of the ALD seed MnO_2 layer and Ni film electroplating enable conformal thick EMD coating on high-aspect ratio structures. Figure 10 shows thick conformal EMD deposition on top of high aspect ratio micro-pillars (50 µm high, 2 µm in diameter with 2 µm interpillar spacing) with a 22 nm TiN deposited by ALD and coated by either seed MnO_2 layer with ALD (Figure 10a) or thin Ni layer by electroplating (Figure 10b). Similar deposition was also achieved with C-coated Si pillars as demonstrated in our earlier work.[26] Ability to conformally coat high-aspect ratio structures opens up a variety of new applications of EMD material, including Li-ion batteries with increased battery capacity due to surface microstructuring.

Application of thick EMD films for Li-ion intercalation electrodes.—In principle, MnO_2 is by itself suitable as an electrode material in Li-ion batteries. EMD is indeed used in commercial primary lithium batteries, and can be made reversible for thin films.[5] Cyclic voltammetry of activated EMD thin films shows distinctive cathodic current peak for Mn(IV) reduction and Li-ion intercalation at 2.75 V vs. Li^+/Li and an anodic current peak for the re-oxidation

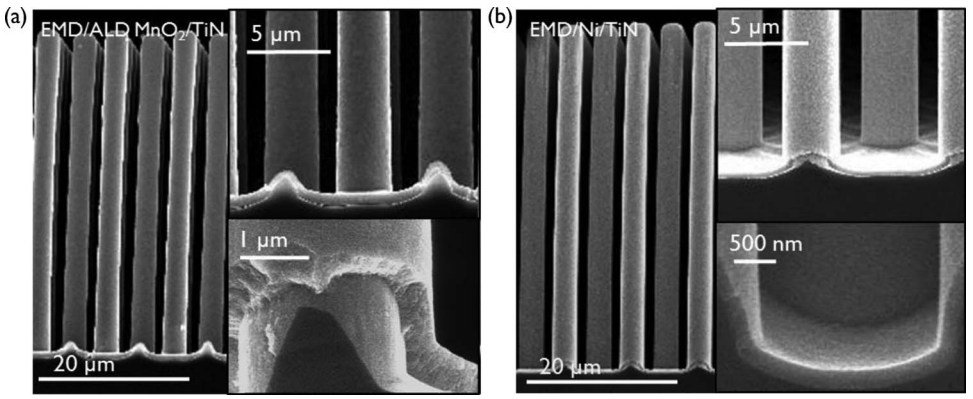

Figure 10. SEM images of conformal thick EMD films electrodeposited on ALD TiN/Si pillars coated with (a) MnO_2 seed layer grown by ALD (EMD coating is ~600 nm), (b) Ni layer grown by electrochemical deposition (EMD coating is ~250 nm). The pillars are 2 µm wide with 2 µm spacing.

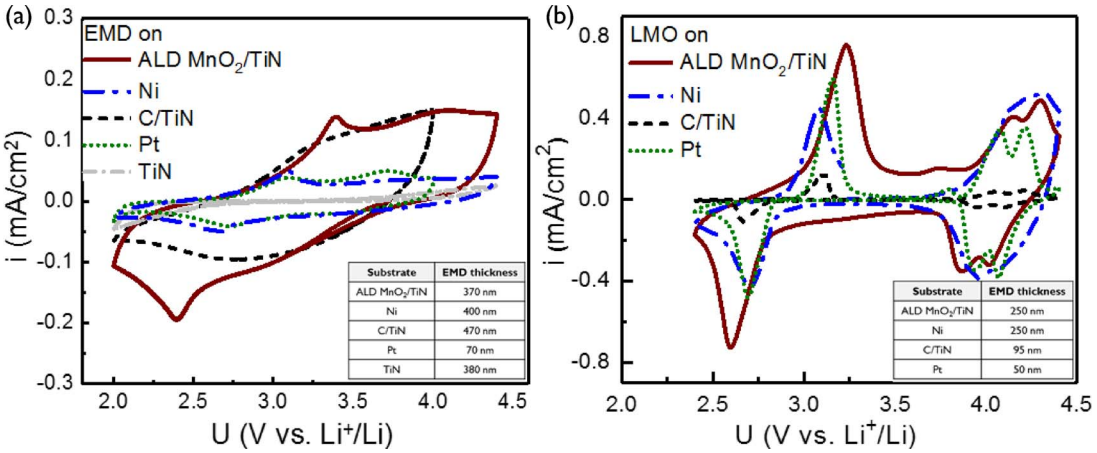

Figure 11. Cyclic voltammograms for Li-ion insertion (cathodic) and extraction (anodic) for (a) as-deposited thick EMD films (50th cycle), (b) EMD films converted to LMO (2nd cycle), on different substrates. The thickness of EMD is shown in the tables at the inset. CVs were measured in 1 M $LiClO_4$ in propylene carbonate at polarization rate of 10 mV/s.

of Mn(III) with Li^+ extraction at 3 V vs. Li^+/Li upon reversing the polarization:[5,9]

$$MnO_2 + xLi^+ + xe^- \leftrightarrow Li_xMnO_2, \text{ with } 0 < x < 1. \quad [6]$$

Activation of the EMD films can be easily done by cycling in the Li-ion electrolyte solution. The improvement in Li^+ intercalation and extraction kinetics of the EMD films upon cycling is attributed to several factors, e.g. changing of the MnO_2 crystal structure with cycling, increased contact between MnO_2 and the electrolyte, reduction of the remaining water content within the EMD structure, doping of the film by Li-ions and hence increased electronic conductivity.[5] This was shown for example for the 70 nm thick EMD films grown on C/TiN substrate.[9]

Unfortunately, only thin (<50 nm) EMD films show good reversible kinetics with sharp Li-ion intercalation and extraction peaks. As opposed to thin films, thicker EMD films display only broad cathodic (at ~3–3.4 V vs. Li^+/Li) and anodic (at ~2.4–2.6 V vs. Li^+/Li) current peaks in their CVs as shown in Figure 11a for EMD films deposited on the different substrates. Such poor electrochemical response with no distinctive Li-ion intercalation peaks but mostly a capacitive behavior, results from the high electronic and ionic resistances of the EMD films which increase with the film thickness, as discussed in more details in our earlier work.[9]

We have thus developed a process to convert electrochemically deposited MnO_2 layer to $LiMn_2O_4$ (LMO) by solid-state reaction, allowing the application of thick EMD films for Li-ion intercalation electrodes.[27] This is achieved by spin-coating a Li_2CO_3 layer on top of the as-prepared porous EMD film. The solid-state reaction occurs upon annealing with the thermal budget and the amount of MnO_2 and Li_2CO_3 materials optimized in order to fabricate a stoichiometric $LiMn_2O_4$ film according to the following reaction:

$$4MnO_2 + Li_2CO_3 \rightarrow 2LiMn_2O_4 + CO_2 + 1/2O_2 \quad [7]$$

The MnO_2 conversion to $LiMn_2O_4$ using Li_2CO_3 was first demonstrated using a Pt current collector which allowed such high annealing temperatures as 750°C. In this case thin EMD films of 50–70 nm were used due to the limitation to deposit well-adherent thicker EMD films on Pt. The CV of as-fabricated LMO film shows the typical Li-ion insertion and extraction peaks in/from $LiMn_2O_4$ at around 3 and 4 V vs. Li^+/Li, as demonstrated in Figure 11b. The electrode reactions are described as follow:

$$3\text{ V region:} \quad LiMn_2O_4 + Li^+ + e^- \leftrightarrow Li_2Mn_2O_4 \quad [8]$$

$$4\text{ V region:} \quad Mn_2O_4 + Li^+ + e^- \leftrightarrow LiMn_2O_4 \quad [9]$$

The capacity of the converted 50 nm film calculated from the CV in the voltage range of 2.4–4.4 V vs. Li^+/Li was found to be equal to 75% of the LMO's theoretical capacity (theoretical capacity = 1.26 Ah/cm^3). The cyclic voltammetry measurement was done at 10 mV/s, thus each scan took 200 s which is equivalent to C-rates over 18 C. Additionally, the formation of a crystalline spinel $LiMn_2O_4$ material was confirmed by XRD analysis where $LiMn_2O_4$ diffraction peaks were observed together with the substrate peaks (Figure 12).

Next, the solid-state conversion to LMO was carried out with thick EMD films on the C/TiN, ALD MnO_2/TiN and Ni/TiN current collector substrates. The annealing temperature was reduced from 750°C to 350°C to prevent oxidation of the underlying materials by oxygen or MnO_2. For example, in the case of C-coated TiN substrate lowering the applied thermal budget was important to prevent MnO_2 reduction by the carbon at higher temperatures, rendering the material inactive. The annealing time was varied in accordance with the thickness of the EMD film. Thus, solid-state conversion reaction was carried out for

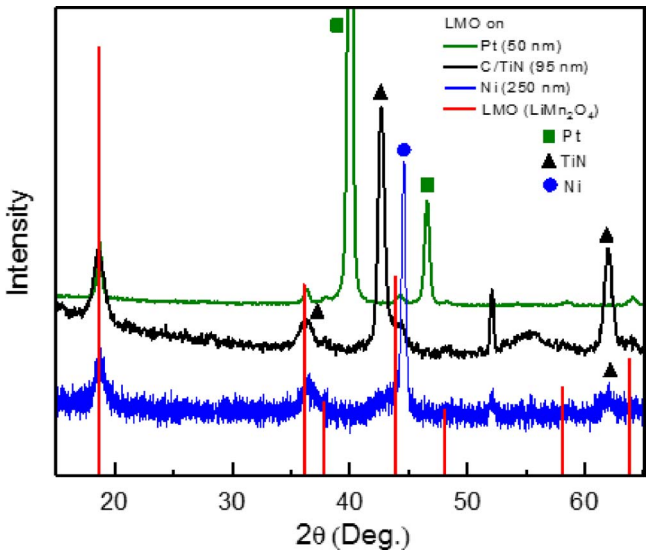

Figure 12. XRD patterns of $LiMn_2O_4$ (LMO) films obtained by converting the EMD layer on Pt/TiN (top, green), C/TiN (middle, black) and Ni/TiN (bottom, blue) substrates. A peak at 2θ = 50–53° is a typical substrate peak given by Si(xyz) plane in Si(tuv) substrate and can be removed by rotating the sample.

Table I. Summary of the test conditions for the conversion of EMD to LMO on different current collector substrates.

current collector interface	EMD thickness	Conversion conditions	LMO capacity
Pt/TiN	50 nm	750°C, 20 min	0.95 Ah/cm^3
C/TiN	95 nm	350°C, 10 min	0.13 Ah/cm^3
ALD MnO_2/TiN	250 nm	250°C, 6 hrs	0.55 Ah/cm^3
Ni/TiN	250 nm	350°C. 120 min	0.43 Ah/cm^3

10 min at 350°C in air for a 95 nm starting EMD film on C/TiN, while for a 250 nm EMD film on Ni/TiN the annealing time was increased to 120 min in air. In case of converting EMD on ALD MnO_2/TiN current collector, the annealing temperature of the Li_2CO_3/EMD/MnO_2/TiN stack was further reduced to 250°C in order to prevent reaction between MnO_2 and TiN with TiN oxidation and reduction of the MnO_2 seed layer. In this specific case, the annealing time was increased to 6 hrs in order to allow enough time for the solid-state reaction with the 250 nm EMD film to occur. Table I summarizes the test conditions of the conversion process on different current collector substrates.

The CVs of as-converted EMD films show the Li-ion insertion/extraction peaks in/from LMO at around 3 and 4 V vs. Li^+/Li, demonstrating a successful conversion on all the substrates (see Figure 11b). The formation of crystalline LMO material was confirmed by XRD (Figure 12). The ERD results of all the samples after annealing indicate that the fabricated LMO film has a stoichiometry close to the theoretical stoichiometry of $LiMn_2O_4$ (Li 14%; Mn 29%; O 57%), e.g. in case of as-fabricated LMO on Pt the stoichiometry was as follows: Li 14%; Mn 24%; O 62%, or in case of as-fabricated LMO on Ni the stoichiometry was Li 13%; Mn 33%; O 54%.

The performance of the LMO films was assessed from the capacity integrated under the CVs. The capacity of the converted EMD films on C/TiN with only 10% of the theoretical capacity was the lowest of all films (i.e. 0.13 Ah/cm^3). Even though the activity of the film converted at 350°C was significantly better than those treated at higher temperatures, the reduction of MnO_2 by the underlying graphitic carbon still seems to be an issue. The highest total capacity was obtained for the films on ALD MnO_2/TiN and Ni/TiN with 44% of the theoretical capacity (0.55 Ah/cm^3) and 34% of the theoretical capacity (0.43 Ah/cm^3), respectively. The lower accessible capacity compared to the converted LMO film on Pt is due to the difference in film thickness, i.e. 50 nm of EMD on Pt versus 250 nm of EMD on ALD MnO_2/TiN and Ni/TiN. The longer heat-treatment of 6 h (at 250°C) for ALD MnO_2/TiN substrate compared to 2 h (at 350°C) for Ni/TiN substrate is believed to be responsible for the larger capacitance on ALD MnO_2/TiN substrate. These results demonstrate the feasibility of the conversion process of EMD films to adherent and active LMO films with submicron to micron thickness on different substrates. Further development is underway to fabricate conformal LMO films also on the microstructured current collectors for 3D thin-film Li-ion battery devices.

Conclusions

A methodology for the electrodeposition of MnO_2 films onto easily oxidizable and technologically-relevant current collectors for 3D energy storage applications is proposed. Anodic electrodeposition of thick and electrochemically active EMD films from conventional acidic $MnSO_4$ electrolyte solutions is not possible on easy to oxidize substrates like TiN due to its passivation or Ni due to its oxidation and dissolution. Optimization of the current collector interface by introducing a non-corrosive protection layer such as carbon film or a dense MnO_2 seed layer allowed to deposit thick EMD films up to 1.3 μm on TiN surfaces with a good adhesion. The use of neutral and complexing acetate bath allowed thick EMD deposition on a Ni surface. The mechanism of EMD growth and film morphology were examined. Compatibility of the proposed approach for the electrodeposition of conformal thick EMD films on 3D high-aspect ratio micropillars was demonstrated. As-grown thick and porous EMD films plated directly on a current collector were shown to be applicable as Li-ion intercalation electrodes upon their conversion to LMO films. The method of solid-state conversion of EMD films to high capacity LMO material on different substrates at low-temperature was demonstrated, paving the way toward their application in 3D Li-ion batteries.

Acknowledgments

The authors acknowledge Alfonso Sepulveda (imec) and Nathalie Hendrickx (imec) for SEM examinations, Marleen van der Veen (imec) for HRSEM images, Johan Meersschaut (imec) for RBS measurements, Olivier Richard (imec) for TEM analysis, Thierry Conard (imec) and Brecht Put (imec) for XPS contributions. This work was partly supported by IWT-Flanders (Belgium) under SBO project "SOS-Lion" (18142).

References

1. D. R. Rolison et al. "Multifunctional 3D nanoarchitectures for energy storage and conversion." *Chem. Soc. Rev.*, **38**, 226 (2009).
2. P. M. Vereecken and C. Huyghebaert, Solid-state battery and method for manufacturing thereof, Imec Vzw, Pat. no. US20140363744A1, EP2814091A1 (2014).
3. E. Eustache, C. Douard, R. Retoux, and C. Lethien, "MnO_2 thin films on 3D scaffold: microsupercapacitor electrodes competing with 'bulk' carbon electrodes." *Adv. Energy Mater.*, **1500680** (2015).
4. B. L. Ellis, P. Knauth, and T. Djenizian, "Three-dimensional self-supported metal oxides for advanced energy storage." *Adv. Mater.*, **26**, 3368 (2014).
5. A. S. Etman, A. Radisic, M. M. Emara, C. Huyghebaert, and P. M. Vereecken, "Effect of film morphology on the Li ion intercalation kinetics in anodic porous manganese dioxide thin films." *J. Phys. Chem. C*, **118**, 9889 (2014).
6. A. Biswal, B. C. Tripathy, K. Sanjay, T. Subbaiah, and M. Minakshi, "Electrolytic manganese dioxide (EMD): a perspective on worldwide production, reserves and its role in electrochemistry." *RSC Adv*, **5**, 58255 (2015).
7. J. Prabhakar Rethinaraj and S. Visvanathan, "Anodes for the preparation of EMD and application of manganese dioxide coated anodes for electrochemicals." *Mater. Chem. Phys.*, **27**, 337 (1991).
8. P. M. Vereecken and C. Huyghebaert, "Conformal deposition for 3D thin-film batteries (Invited)." *ECS Trans*, **58**, 111 (2013).
9. S. Deheryan et al. "Nanometer-thin graphitic carbon buffer layers for electrolytic MnO_2 for thin-film energy storage devices." *J. Electrochem. Soc.*, **164**, A538 (2017).
10. M. F. DuPont and S. W. Donne, "Nucleation and growth of electrodeposited manganese dioxide for electrochemical capacitors." *Electrochim. Acta*, **120**, 219 (2014).
11. A. J. Gibson, B. Johannessen, Y. Beyad, J. Allen, and S. W. Donne, "Dynamic electrodeposition of manganese dioxide: temporal variation in the electrodeposition mechanism." *J. Electrochem. Soc.*, **163** (2016).
12. W. M. Dose, J. Lehr, and S. W. Donne, "Characterisation of chemically lithiated heat-treated electrolytic manganese dioxide." *Mater. Res. Bull.*, **47**, 1827 (2012).
13. Y. Qiu et al. "Electrodeposition of manganese dioxide film on activated carbon paper and its application in supercapacitors with high rate capability." *RSC Adv*, **4**, 64187 (2014).
14. J. Xiao, S. Yang, L. Wan, F. Xiao, and S. Wang, "Electrodeposition of manganese oxide nanosheets on a continuous three-dimensional nickel porous scaffold for high performance electrochemical capacitors." *J. Power Sources*, **245**, 1027 (2014).
15. L. Baggetto, R. Niessen, F. Roozehoom, and P. H. L. Notten, "High energy density all-solid-state batteries: A challenging concept toward 3D integration." *Adv. Funct. Mater.*, **18**, 1057 (2008).
16. H. Zhang, X. Yu, and P. V. Braun, "Three-dimensional bicontinuous ultrafast-charge and -discharge bulk battery electrodes." *Nat. Nanotechnol.*, **6**, 277 (2011).
17. O. Nilsen, H. Fjellvag, and A. Kjekshus, "Growth of manganese oxide thin films by atomic layer deposition." *Thin Solid Films*, **444**, 44 (2003).
18. F. Mattelaer, P. Vereecken, J. Dendooven, and C. Detavernier, "Deposition of MnO anode and MnO_2 cathode thin films by plasma enhanced atomic layer deposition using the $Mn(thd)_3$ precursor." *Chem. Mater.*, **27,10**, 3628 (2015).
19. J. Dendooven, D. Deduytsche, J. Musschoot, R. L. Vanmeirhaeghe, and C. Detavernier, "Conformality of Al_2O_3 and AlN deposited by plasma-enhanced atomic layer deposition." *J. Electrochem. Soc.*, **157**, G111 (2010).
20. W. Knaepen, C. Detavernier, R. L. Van Meirhaeghe, J. Jordan Sweet, and C. Lavoie, "In-situ X-ray diffraction study of metal induced crystallization of amorphous silicon." *Thin Solid Films*, **516**, 4946 (2008).

21. F. Mattelaer et al. "Manganese oxide films with controlled oxidation state for water splitting devices through a combination of atomic layer deposition and post-deposition annealing." *RCS Adv*, **6**, 98337 (2016).
22. R. L. Paul and A. Cartwright, "The mechanism of the deposition of manganese dioxide." *J. Electroanal. Chem.*, **201**, 113 (1986).
23. C. J. Clarke, G. J. Browning, and S. W. Donne, "An RDE and RRDE study into the electrodeposition of manganese dioxide." *Electrochim. Acta*, **51**, 5773 (2006).
24. H. G. G. Philipsen et al. "Through-silicon via technology for 3D applications." *ECS Trans*, **25**, 97 (2010).
25. R. Akolkar, "Characterizing transport limitations during copper electrodeposition of high aspect ratio through-silicon vias." *ECS Electrochem. Lett.*, **2**, 6 (2013).
26. Y. Zargouni, S. Deheryan, A. Radisic, K. Alouani, and P. Vereecken, "Electrolytic manganese dioxide coatings on high aspect ratio micro-pillar arrays for 3D thin film lithium ion batteries." *Nanomaterials*, **7**, 126 (2017).
27. N. Labyedh, M. Y. Timmermans, and P. M. Vereecken, "Methods for forming Lithium Manganese Oxide layers." US 2017/0125789 Al (2017).